Pol. J. Environ. Stud. Vol. 22, No. 1 (2013), 7-24

Review

Sorptive Interaction of Oxyanions with Iron Oxides: A Review

Haleemat Iyabode Adegoke[1]*, Folahan Amoo Adekola[1], Olalekan Siyanbola Fatoki[2], Bhekumusa Jabulani Ximba[2]

[1]Department of Chemistry, University of Ilorin P.M.B. 1515, Ilorin, Nigeria
[2]Department of Chemistry, Faculty of Applied Sciences, Cape Peninsula University of Technology, P.O. Box 652, Cape Town, South Africa

Received: 5 December 2011
Accepted: 24 July 2012

Abstract

Iron oxides are a group of minerals composed of Fe together with O and/or OH. They have high points of zero charge, making them positively charged over most soil pH ranges. Iron oxides also have relatively high surface areas and a high density of surface functional groups for ligand exchange reactions. In recent time, many studies have been undertaken on the use of iron oxides to remove harmful oxyanions such as chromate, arsenate, phosphate, and vanadate, etc., from aqueous solutions and contaminated waters via surface adsorption on the iron oxide surface structure. This review article provides an overview of synthesis methods, characterization, and sorption behaviours of different iron oxides with various oxyanions. The influence of thermodynamic and kinetic parameters on the adsorption process is appraised.

Keywords: oxyanions, iron oxides, adsorption, isotherm, points of zero charge

Introduction

Iron oxides are a group of minerals composed of iron and oxygen and/or hydroxide. They are widespread in nature and are found in soils and rocks, lakes and rivers, on the seafloor, in air, and in organisms. Iron oxides are of great significance for many of the processes taking place in the ecosystem. They are ubiquitous in soils and sediments, where they are important regulators of the concentration and distribution of plant nutrients and pollutants such as heavy metals [1]. Iron oxides can be both beneficial and undesirable. There are 17 known iron oxides differing in composition, valence of Fe, and – most importantly – in crystal structure [2]. Iron oxides have been studied for their potential use in a wide range of important uses such as pigments in ceramic glaze, catalysis, electrochemistry, magnetization, biomedical science, and environmental applications [3-8].

*e-mail: ihalimat@yahoo.com

Iron oxides have been used as catalysts in the chemical industry [9, 10], and a potential photoanode for possible electrochemical cells [11, 12]. In medical applications, nanoparticle magnetic and superparamagnetic iron oxides have been used for drug delivery in the treatment of cancer [13, 14]. There also has been considerable interest in using iron oxides to remove environmental contaminants since environmental pollution has emerged as an important issue in recent decades. Increasing interest has recently been diverted to evaluating the ability of iron oxides to remove contaminants such as arsenite, arsenate, chromate, vanadate, and phosphate etc., from aqueous solution by the process of adsorption. This is because iron oxides have exhibited a great potential to efficiently remove harmful oxyanions due to the earlier-mentioned characteristic of high surface area.

The aim of this review is therefore to discuss iron oxide composition and structure, synthesis and characterization with specific emphasis on their ability to adsorb oxyanions

from aqueous solution. Several factors that play important roles in the adsorption process, such as pH, competitive anions, temperature, and particle size, will also be discussed in light of literature results.

Composition and Structure of Iron Oxides

Most of the iron oxides contain Fe (III); only in FeO and $Fe(OH)_2$ is iron exclusively present in the divalent state, whole green rusts and magnetite are mixed Fe (II) – Fe (III) minerals. There are five polymorphs of FeOOH and four of Fe_2O_3. Nearly all iron oxides are crystalline (with the exception of ferrihydrite and schwermannite, which are poorly crystalline). The degree of crystal order is, however, variable and depends on the conditions under which the iron oxides are formed [2]. Table 1 shows an overview of different iron oxides, hydroxides, and oxy-hydroxides.

Iron oxides consist of arrays of iron and oxygen or hydroxides. Since oxygen and hydroxides are much larger than the iron atoms, the crystal structure of the oxides is controlled by the arrangement of the oxygens and hydroxides. The sheets of oxygen and hydroxide are most commonly stacked ABAB. (hexagonal close packing, or hcp) or ABCABC. (cubic close packing, or ccp), while Fe is placed in the interstices between the oxygen and hydroxide sheets. To fulfill the charge balance requirement, only part of the interstices is filled with Fe. The various iron oxides differ in the arrangement of Fe in the interstices, and to a lesser extent differences in the stacking of oxygen and hydroxide sheets [2].

Fe is predominantly octahedrally (FeO_6 or $FeO_3(OH)_3$), and in some cases tetrahedrally (FeO_4) coordinated in the iron oxides, and the resultant octahedral and tetrahedral constitute the basic structural unit of iron oxides. An alternative way of considering the iron oxide crystal structure is the linkage of these basic structural units, since the linkage by sharing either corners, edges, or faces results in different iron oxides. Figs. 1 a-c show the structure of goethite, hematite, and magnetite according to Ghose et al. [15].

Properties and Uses of Iron Oxides

Iron (II) oxide (FeO) or ferrous oxide is also known as wustite in its mineral form. As a powder, this black oxide can cause an explosion as it readily ignites. Iron (III) oxide (Fe_2O_3) or ferric oxide is also known as hematite (alpha form) or maghemite (gamma form) in its mineral form. As an industrial chemical it is commonly called 'rouge' or red. In a dry or alkaline environment, it can cause passivation and inhibit rust. Iron (II,III) oxide (Fe_3O_4) or ferrous ferric oxide is also known as magnetite or lodestone in its mineral form. Magnetite forms readily when iron oxidizes under water, and so it is often found inside tanks or below the waterline of ships. Color is one of the most striking features of the iron oxides. Iron oxides are responsible for the vivid colors of rocks and soils. The most common shades are red, brown, and yellow, but purple, black (magnetite) and even greenish blue (green rust) also occur. Due to their color (and also their opacity and light fastness), natural iron oxides have been used for decoration since prehistoric times [1]. The most industrially important iron ores are chemically iron oxides. Some iron oxides are widely used in ceramic applications, particularly in glazing. Many metal oxides provide the colors in glazes after being fired at high temperatures. Iron (II) oxide is black, while iron (III) oxide is red or rust colored. Iron compounds other than oxides can have other colors. Iron oxides yield pigments, and natural iron oxide pigments are called 'ochre.' Many classic paint colors, such as raw and burnt siennas and umbers, are iron oxide pigments. These pigments have been used in art since prehistoric times. Iron pigments are also widely used in the cosmetic field. They are considered to be non-toxic, moisture-resistant, and non-bleeding. Iron oxides graded safe for cosmetic use are produced synthetically in order to avoid the inclusion of ferrous or ferric oxides and impurities normally found in naturally occurring iron oxides. The iron oxide cycle (Fe_3O_4/FeO) is a two-step thermo-chemical process used for hydrogen production [2].

Table 1. Overview of iron oxides.

Oxides-hydroxides and hydroxides	Oxides
Goethite (α-FeOOH)	Wüstite (FeO)
Akaganéite (β-FeOOH)	Magnetite (Fe_3O_4)
Lepidocrocite (γ-FeOOH)	Hematite (α-Fe_2O_3)
Feroxyhyte (δ'-FeOOH)	Maghemite (γ-Fe_2O_3)
- (δ-FeOOH)	- (β-Fe_2O_3)
Ferrihydrite ($Fe_5HO_8{\cdot}4H_2O$)	- (ε- Fe_2O_3)
High-pressure FeOOH	
Benalite $Fe(OH)_3$	
- $Fe(OH)_2$	
Schwertmannite $Fe_{16}O_{16}(OH)_y$	
$(SO_4)_z{\cdot}nH_2O$	
Green Rusts $Fe_x^{III}Fe_y^{II}(OH)_{3x+2y-z}(A^-)_z$; $A^- = Cl^-$; $½SO_4^{2-}$	

Synthesis of Iron Oxides

Iron oxides can be regarded as a class of minerals that are simple to synthesize in the laboratory, although not always as pure phases. In general, there are several approaches to preparing iron oxides. Recently, a thorough review has been prepared by Cornell and Schwertmann [1] on the preparation of iron oxides. The preparation and properties of iron oxides continue to attract considerable interest and attention because of their importance in magnetic mate-

rials technology [16]. The formation of iron oxides in an aqueous system involves nucleation and crystal growth [4]. Nucleation is classified into homogeneous nucleation and heterogeneous nucleation. Homogeneous nucleation occurs spontaneously in bulk solution when the supersaturation (i.e ion activity product of a certain compound exceeds its solubility product) exceeds a certain critical value. The formation of stable embryonic clusters of molecules or ions (nuclei) in solution is the essential requirement for precipitation to occur [1]. Heterogeneous nucleation thus occurs when the presence of a solid phase reduces the free energy of nucleation and thus leads to an increase in the rate of nucleation. The substrate may be minute particles of foreign phase or crystals (seeds) of the phase that is crystallizing. Heterogeneous nucleation can take place at a lower level of supersaturation than is required for homogeneous nucleation [1].

In crystal growth a certain degree of supersaturation is required but it is much less than that needed for nucleation. Crystal growth may be controlled either by transport process or by surface chemical reaction. The mechanism by which a crystal grows may depend on some conditions. Changes in the degree of supersaturation or solution variables may lead to a change in mechanism during growth. The nature of a crystal is governed by the rate of growth of its different faces. Those faces that grow slowly tend to persist in the crystal, whereas fast-growing faces are eliminated. The crystal habit/nature is therefore determined primarily by the slow-growing faces. Adsorbing foreign ions may alter the rate at which different crystal faces grow and modify the habit of crystal [1].

Almost all the iron oxides and hydroxides can be prepared by a number of synthesis routes. The method of synthesis frequently influences the properties of the product, particularly crystal morphology, degree of crystallinity, sample surface area and water content. The synthesis methods proposed by Cornell and Schwertmann [1] are: hydrolysis of acidic solution of Fe(III) salts, transformation of ferrihydrite in alkaline media, oxidative hydrolysis, phase transformation, and decomposition of metal chelates.

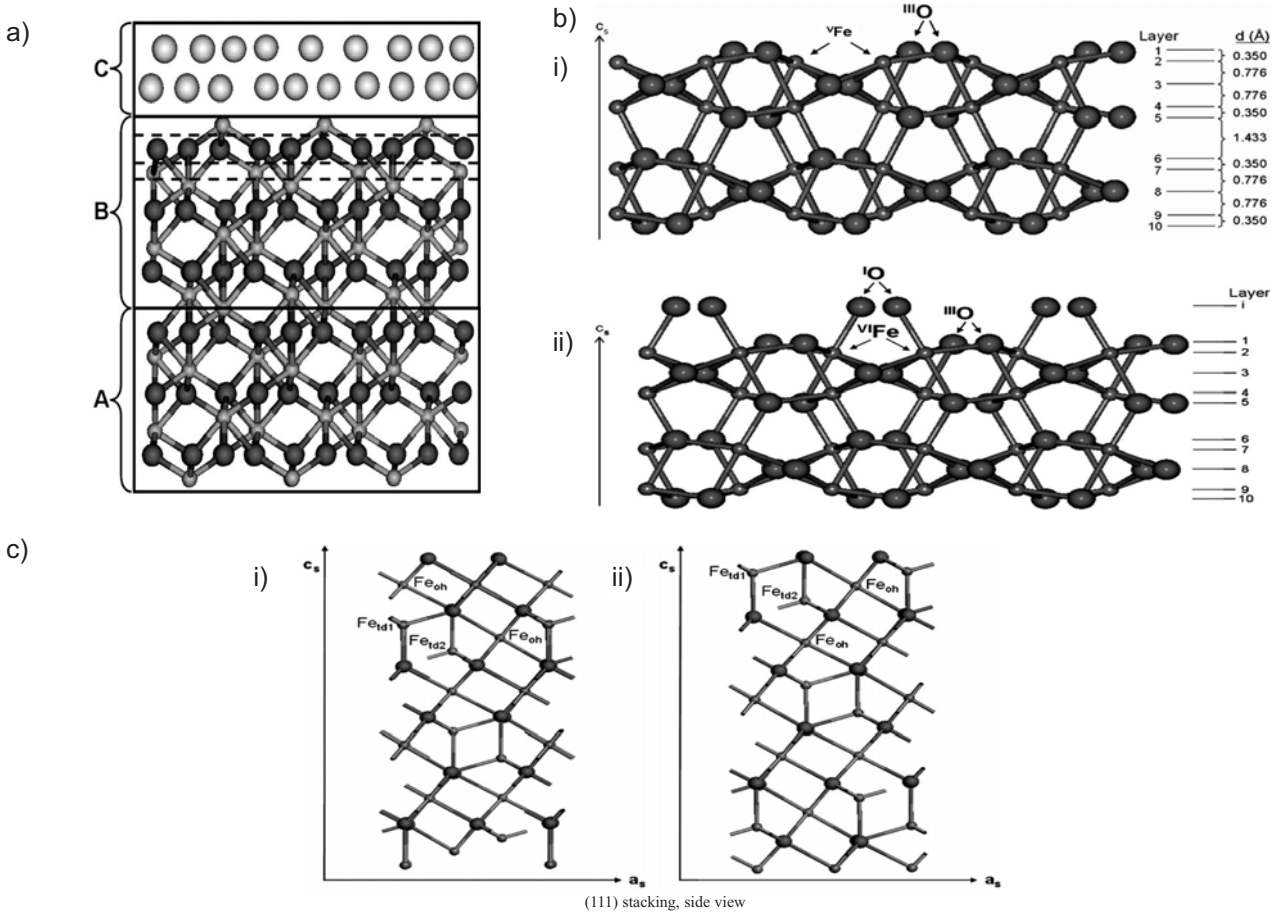

Fig. 1. a) Structure of Goethite α-FeOOH (1 0 0) – water interface. A schematic picture of the atomic layer model for CTR analysis: A – crystalline bulk structure, B – crystalline surface structure, and C – semi-ordered physisorbed water or sorbates (Ghose et al.) [15]; b) Structure of Hematite α-Fe_2O_3 (1102) – water interface. Layer Stacking Sequence Along cs Axis for α-Fe_2O (1 $\bar{1}$ 0 2); (i) ideal bulk stoichiometric termination and (ii) hydroxylated stoichiometric termination. The large spheres represent oxygen and small spheres represent iron atoms. The ^{I}O and ^{III}O represent oxygen atoms coordinated to one and three iron atoms, respectively, and the ^{V}Fe and ^{VI}Fe represent iron atoms coordinated to five and six oxygen atoms, respectively (Ghose et al.) [15]. c) Structure of magnetite Fe_3O_4 (1 1 1) – water interface. Layer stacking sequence along the cs axis for the oxygen terminated Fe_3O_4 (1 1 1) (i) O4-Feoh-O4-Fetd1_oh_td2 and (ii) O4-Fetd1_oh_td2-O4-Feoh where the large spheres represent oxygen atoms and the small spheres represent iron atoms (Ghose et al. [15]).

Hydrolysis of Acidic Solution of Fe(III) Salts

At very low pH (<1) Fe^{3+} exists as a purple hexa –aquo ion, $[Fe(H_2O)_6]^{3+}$. Hydrolysis involves the stepwise elimination of the proton from the six water molecules that surround the central Fe cation to form mono and bi nuclear species, which interact further to produce species of higher nuclearity [17]. The polymeric species eventually precipitate. The condition of crystallinity of the precipitate depends on the reaction conditions. Precipitation time may range from seconds to years.

Examples of hydrolysis reactions are:

$$Fe^{3+} + H_2O \rightarrow FeOH^{2+} + H^+ \quad (1)$$

$$Fe^{3+} + 2H_2O \rightarrow Fe(OH)_2^+ + 2H^+ \quad (2)$$

$$Fe^{3+} + 2H_2O \rightarrow FeOOH + 3H^+ \quad (3)$$

$$2Fe^{3+} + 3H_2O \rightarrow Fe_2O_3 + H^+ \quad (4)$$

Heating of solution and the addition of base are the two principal methods used to induce hydrolysis in the laboratory.

As hydrolysis releases protons, pH of the system falls during the early stages of hydrolysis. pH may fall to a low enough value to inhibit further hydrolysis in cases where hydrolysis is induced by raising the temperature. The pH drop is important because incomplete hydrolysis reduces the yield of products [1].

Hematite, akaganeite, and ferrihydrite may be obtained by hydrolysis of Fe^{3+} solutions. The product formed is influenced by a variety of factors, including rate of hydrolysis, pH of the solution, temperature, concentration of Fe^{3+}, and the nature of anion present. The reaction condition must be carefully controlled in order not to obtain mixtures, rather than a single product. Some researchers have investigated the synthesis method intensively and have shown the various ways in which the reaction product and also morphology may be influenced by reaction conditions [18, 19].

The most important application of the acidic hydrolysis method is in the production of hematite and akaganeite, but goethite can also be synthesized in this way [1]. Low product yield is the disadvantage of the method. Ramming et al. also reported the synthesis of nanosized super paramagnetic hematite using hydrolysis reaction [20]. A well-defined subrounded morphology hematite was obtained with an average diameter of 41 nm particle size. The synthesis of iron oxides by hydrolysis reaction using the hydrothermal method have been reported recently [21]. In this study single crystalline α-Fe_2O_3 nanocubes were successfully obtained in large quantities through a facile one-step hydrothermal synthesis route under mild conditions. The products were characterized by powder X-ray diffraction (XRD), scanning electron microscopy (SEM), high resolution transmission electron microscopy (HRTEM), select-area electron diffraction (SAED), and Fourier transform infrared spectrometry (FTIR) [21].

Transformation of Ferrihydrite in Alkaline Media

Ferrihydrite is the initial product resulting from fast hydrolysis (by addition of alkali) of an Fe^{3+} salt solution (2-line ferrihydrite). It is thermodynamically unstable and transforms into goethite, hematite or a mixture of the two with time. These compounds formed by different pathways. The formation of hematite, involves an internal dehydration/rearrangement process within the particles of ferrihydrite, whereas the formation of goethite proceeds via dissolution of ferrihydrite followed by nucleation and growth of crystalline phase [22, 23]. Both processes take place only in the presence of water. Hematite formation is promoted by factors that induce aggregation of ferrihydrite particles (pH near the PZC ferrihydrite, i.e pH 7-8) or dehydration (i.e increased temperature) [24]. The transformation to goethite is the dissolution/reprecipitation process in which the reaction rate is governed by the rate of dissolution of ferrihydrite or nucleation of crystal growth of goethite. The formation of goethite is favoured by raising or lowering the pH away from the PZC because this promotes dissolution of ferrihydrite [25]. A plot of transformation of ferrihydrite into goethite or hematite versus time displays an initial induction period to the nucleation of the product followed by a faster stage that is first-order with respect to the amount of precursor remaining in the system [23].

Oxidative Hydrolysis of Fe(II) Salts

This is a very versatile method capable of producing goethite, lepidocrocite, magnetite, ferrihydrite, and feroxyhyte. The product formed depends on the reaction conditions, on particular pH, rate of oxidation, suspension concentration, temperature, and concentration of foreign species [26, 27]. An inert atmosphere of nitrogen must be provided for production [28]. The reaction can be carried out over the pH range 6-14. Between pH 6-7, goethite and lepidocrocite are formed; pure products of either can be obtained by adjusting the rate of oxidation and concentration of the carbonate in the system [27, 28]. Magnetite is obtained at pH >8 and pure goethite is produced at pH 14. Feroxyhyte is obtained with very rapid oxidation (e.g. using H_2O_2).

The oxidation/hydrolysis reaction releases protons so that as the transformation proceeds, the pH drops to about 3 and the transformation rate falls to practically zero (if no extra base is added), hence oxidation is complete:

$$2Fe^{2+} + 3H_2O + 1/2O_2 \rightarrow 2FeOOH + 4H^+ \quad (5)$$

pH must be held constant by the continual addition of alkali to the system in order to obtain a higher yield of reasonable crystalline product. This is most conveniently achieved by using an automatic burette and pH-stat titration technique. The reaction is complete when the further addition of alkali is required [1]. An alternative method is the use of buffer ($NaHCO_3$ or imidazole), but the end product will be contaminated. A feature of the oxidation/hydrolysis of Fe^{2+} systems is that a crystalline product can be obtained between a few hours at room temperature.

Phase Transformations

Phase transformation refers to conversion of one crystalline iron oxide or oxyhydroxide into another under suitable conditions. Every iron oxide can be converted into at least one other member of the groups [29]. The products frequently retain the crystal morphology of the starting material (pseudomorphosis) where a topotactic transformation mechanism is involved: for example, the formation of maghemite by thermal dehydration of lepidocrocite or by oxidation of magnetite and also the formation of hematite at moderate temperature (200ºC) via thermal dehydration of goethite [1].

Decomposition of Metal Chelates

Decomposition of Fe (III) chelates is a suitable technique for the production of fairly monodispersed products (often with unusual morphologies) because it provides a constant and controlled supply of reactant [30]. The reaction is carried out at temperatures greater than 100ºC and pH above 12. This method has been used to produce hematite and magnetite. The nature of the product in terms of the shape and size of the crystals are governed by the type of additives in the system. A disadvantage of this method is that the product may be contaminated by the ligand.

The sol gel method has also been reported for the synthesis of iron oxides. Duhan and Devi synthesized nanosized (20-42 nm) iron oxide powders using the solgel method at 700ºC [31]. Gong et al. reported the synthesis of continuous hollow α-Fe_2O_3 fibers by sol gel method using ferric alkoxide and acetic acid as the starting materials and alcohol as the solvent [32]. Holland and Yamaura also reported the synthesis of nanoparticle magnetite by precipitation method [33]. The precipitation was carried out by heating the mixture in a boiling water bath and a domestic microwave oven. Their product was characterized by SEM, XRD, and FTIR. Parsons et al. synthesized iron oxide/oxyhydroxide using the microwave-assisted method [34]. The experiment was conducted by using iron (III) chloride titrated with sodium hydroxide at different temperatures from 100-250ºC. The particles were characterized using TEM, XRD and XAS (x-ray absorption spectroscopy). The average particle sizes of the nanoparticles synthesized were in the range 17-33 nm [34]. A simple reduction-oxidation method also has been reported for the synthesizing plate-shaped γ-Fe_2O_3 nanocrystals at room temperature and under ambient pressure. The reaction was carried out in two steps: Fe (II) was reduced to Fe atoms by γ-ray irradiation in nitrogen atmosphere in the first step while Fe atoms were oxidized into γ-Fe_2O_3 in air [35].

Characterization of Iron Oxides

Iron oxides consist of crystals ranging in size from 0.01 nm to several μm; they are characterized and checked for purity by the techniques commonly used for submicroscopic particles. The most important techniques are x-ray powder diffraction and electron microscopy. In addition, Mossbauer spectroscopy, infrared absorption spectroscopy, and thermal analysis give complimentary useful information [36]. All iron oxides have vivid colors that can be used for their characterization.

X-ray powder diffraction is essential for identification and purity control of the product. In addition, it may provide information concerning crystal size and disorder, structural parameters (unit cell edge lengths), degree of Isomorphous substitution, and surface area. The minimum size required for a crystallite to diffract x-rays is in the range of a few cells (ca 2-3 nm) [1]. Usually the x-ray pattern is recorded as a diffractogram using a goniometer equipped with a proportional or scintillation counter and a registration unit. Occasionally, film cameras, such as the Guinier camera, may be used. The common type of x-ray radiation normally used for Fe oxides are CoK∞ or FeK∞ radiation with a wavelength of 0.178890 and 0.193604 nm, respectively.

Electron microscopy is also a technique that enables crystal dimensions and also morphology to be measured directly. It is also useful for indicating the presence of amorphous material or traces of iron oxides not detectable by XRD. For example, transmission electron microscopy revealed the presence of a few percent fine needles of goethite in a preparation that, according to XRD, consisted of hematite only.

Mossbauer spectroscopy is a very useful tool in studies of local interactions between nuclear probes contained in the material investigated and their nearest environment [37]. The sensitivity of Mossbauer spectroscopy is substantially higher than XRD; it allows phases invisible to XRD to be revealed [38]. Mossbauer spectroscopy can be used for quantitative analysis of mixtures of different phases.

Infra red spectroscopy provides a rapid method of identification if the iron oxide is crystalline. It is also useful for detecting traces (1-2%) of goethite in a hematite preparation [1]. This technique enables detection of low levels of impurities arising from the preparation procedure and not washed out of the product. Such impurities include nitrate (~1400 cm^{-1}) and carbonate (~1300 and ~1500 cm^{-1}) [4]. The most suitable procedure for examination involves the use of KBr tablets consisting of 0.5-2 mg iron oxide and 300 mg pure KBr. Too much iron oxide in the tablet leads to a poor spectrum.

Thermogravimetry analysis (TGA) is a technique that provides information about absorbed and structural water present in iron oxides and also about phase specific changes and transformations [1]. A sample is continuously heated at a constant rate (2-10ºC·min^{-1}) and its weight loss is measured using a balance. Fe-oxides containing structural OH, for example goethite and lepidocrocite, lose weight at between 250-400ºC by the dehydroxylation reaction:

$$2OH^- \rightarrow O_2^- \rightarrow H_2O$$

All fine-grained material contains adsorbed water and additional weight loss stems from loss of adsorbed water at a characteristic temperature of between 100º and 200ºC.

Table 2. Zero points of metal (hydr)oxides [43].

Material	Description	Electrolyte	TºC	Method	pH_O	Reference
Fe_2O_3	Hematite, Alfa Aesar	0.03 mol·dm^{-3} NaCl	-	IEP	6.5	Pan et al. [44]
Fe_2O_3	Monodispersed hematite from $FeCl_3$		23	IEP	10	Kirwan et al. [45]
Fe_2O_3	Hematite, natural, heated at 700ºC, 0.68% SiO_2 0.29% AL_2O_3	0-0.001 mol·dm^{-3}	25	IEP	5.8	Das et al. [46]
Fe_2O_3	Synthetic, Commercial Minerals, 99.5%, hematite with admixture of lepidocrocite	0.001 mol·dm^{-3} KNO_3	22	Acousto	5.6	Mensah and Ralston [47]
Fe_2O_3	Hematite, from nitrate	0.003-0.1 mol·dm^{-3} $NaNO_3$	25	Cip	8.8	Peacock and Sherman[48]
Fe_2O_3	Hematite, Synthetic	0.01 mol·dm^{-3} NaCL	25	IEP	8.5	Chibowski et al. [49]
Fe_2O_3	α, from nitrate	0.1 mol·dm^{-3} $NaNO_3$	25	pH	7.5	Jarlbring et al. [50]
Fe_2O_3	γ, from chloride	0.1 mol·dm^{-3} $NaNO_3$	25	PH IEP	6.5 6.2	Jarlbring et al. [50]
Fe_2O_3	From nitrate, hydrous		25	pH	7.6	Fan et al. [51]
$Fe_2O_3 \cdot nH_2O$	From chloride			IEP	5.5	Kreller et al. [52]
$Fe_2O_3 \cdot nH_2O$	From nitrate	0.1 mol·dm^{-3} NaCl		pH	7.7	Davranche et al. [53]
FeOOH	Goethite, from nitrate	0.003-0.1 mol·dm^{-3}	25	CiP	8.5	Peacock and Sherman [54]
FeOOH	Lepidocriate, hydrolysis and oxidation of $FeCl_2$	0.003-0.1 mol·dm^{-3}	25	CiP	7.7	Peacock and Sherman [48]
FeOOH	From nitrate	0.002-0.093 mol·dm^{-3} KNO_3	25	Merge	9.2	Saito et al. [55]
FeOOH	Goethite, from sulfate	0.01 mol·dm^{-3} KNO_3		IEP	8.1	Varanda et al. [56]
FeOOH	Goethite from nitrate 2 samples	0.1 mol·dm^{-3} $NaNO_3$	25	pH	9.2	Boily et al. [57]
FeOOH	Goethite from nitrate	0, 0.1 mol·dm^{-3}	25	IEP	7.8	Juang and Chung [58]
FeOOH	Goethite from nitrate	0.001-0.1 mol·dm^{-3} $NaNO_3$		CiP	8.8	Xu and Axe [59]
FeOOH	Goethite, from nitrate	0.005-0.1 mol·dm^{-3} KNO_3	25	IEP CiP	9.3 9.3	Antelo et al. [60]
FeOOH	Nanoparticles, from chloride			IEP	8.3	Nielsen et al. [61]

CIP – common intersection point of potentiometric titration curves obtained at three or more ionic strengths
Intersection – intersection point of potentiiometric titration curves obtained at two ionic strengths
Merge – the titration curves obtained at different ionic strengths merge below an above a certain pH
pH – natural pH of the dispersion
IEP – Isoelectric point obtained by means of electrophoresis or electroosmosis
Acousto – Isoelectric point obtained by means of the electroacoustic method

Pure oxides such as hematite may, if fine grained, contain some OH in the structure, and this is driven off over a wide temperature range.

In differential thermal analysis (DTA), a sample is continuously heated at a constant rate (~10ºC·min^{-1}) and the temperature difference between an inert compound and the sample is recorded. Differences in temperature occur if reactions are either exothermic or endothermic. These effects are recorded as peaks on a plot of temperature difference versus temperature for Fe oxides. Endothermic effects result from the release of adsorbed or structural water and exothermic effects come from phase transformations (e.g | |-Fe_2O_3, → ∞-Fe_2O_3) or from recrystallization processes involving the transformation of small crystals into larger ones. The latter process is often observed during the transformation of ferrihydrite to hematite [1, 25].

Point of zero charge is also another method of characterizing iron oxides. The pH where the net total particle charge is zero is called the point of zero charge (PZC), which is one of the most important parameters used to describe variable-charge surfaces [39, 40]. PZC is a very important parameter because it characterizes the protonation-deprotonation behavior of various types of solid, mainly that of (hydr) oxides in aqueous suspensions [41]. It is well known that positive or negative surface sites are developed on the surface of solids in aqueous suspensions. The position of the PZC defines the affinity of the surface to the ionic surfactants and polyelectrolytes, which are widely

used to modify the surface properties. The knowledge of the PZC of the materials of interest facilitates the choice of surfactant for a specific purpose, e.g. in mineral processing (floatation) or the choice of an adsorbent for removal of certain solutes (e.g. from waste water) makes it possible to predict the pH effect on the phenomena and processes involving adsorption [42]. Table 2 presents the PZC of some iron (hydr)oxides.

Synthesis and Characterization of Iron Oxides by Different Researchers

Iron oxides such as hematite, goethite, ferrihydrite, and magnetite have been synthesized and characterized by researchers using different methods as earlier mentioned in the preceding discussion. Other reports by different researchers are discussed below.

Wang et al. synthesized well dispersed nanoparticles with a close cage structure hematite (α-Fe_2O_3) by a low temperature hydrothermal method. The final products were investigated by XRD, Raman spectrum, TEM, and field emission scanning electron microscopy [62].

Marek Kosmulski et al. in their study aged synthetic goethite at 140ºC overnight, leading to composite material in which hematite is detectable by Mossbauer spectroscopy, but XRD does not reveal any hematite peaks [37]. Yu and Hui prepared uniform nano-needle hematite particles by forced hydrolysis, namely by reflux of $Fe(NO_3)_3$ solution in the presence of an organic chelating agent, 1-hydroxyethyl-1,1-diphosphonic acid (HEDP) and HNO_3. Nano-needle hematite particles with a length of 90-100 nm and axial ratio of 9-12 were obtained. The effects of concentration of HEDP and HNO_3 on the morphology of the hematite particle were investigated by TEM. They thought the amount of positive charges on the primary particle surface is crucial for the formation of nano-needle particles from the morphology of the particles extracted at different stages of hydrolysis [63].

Li et al prepared ultrafine α-Fe_2O_3 and Fe_3O_4 particles through a hydrothermal process at 150ºC from a $(NH_4)_2SO_4$ and $FeSO_4 \cdot 6H_2O$ solution in the presence of hydrazine. The products were characterized by XRD and TEM and the formation of pure ∞-Fe_2O_3 and Fe_3O_4 powders was strongly influenced by the pH values of the aqueous solution [64].

Sorescu et al. synthesized hematite particles of four different morphologies (polyhedral, platelike, needlelike, and diskshape) by hydrothermal method. The morphology and average particle diameter (1.4, 7.4, 0.2, and 0.12 μm, respectively) were determined by (TEM) combined with electron diffraction. The hematite samples were studied by Mossbauer spectroscopy in the temperature range 4.2-300 K. In all cases, a weak ferromagnetic phase (WF) was present above the Morin temperature (temperature for which the antiferomagnetic phase is reduced to 50% of the value) of 230 k and found to coexist with antiferromagnetic phase (AF) below this temperature. The populations of the two phases at 230 k were demonstrated to depend on the morphology of the particles. The weak ferromagnetic and antiferromagnetic phases exhibited a different dependence of the magnetic texture on temperature and particle morphology [65].

Schwertmann and Murad in their study stored ferrihydrite in aqueous suspension at 24ºC and pH between 2.5 and 12 for as long as three years, resulting in the formation of goethite and hematite. The proportions and crystallinity of these products widely varied with pH. Maximum hematite was formed between pH 7 and 8, and maximum goethite at pH 4 and 12. The crystallinity of both products was indicated by X-ray powder diffraction line broadening and hyperfine field values and distribution widths. The lower the proportion of the corresponding product in the mixture, the poorer the distribution width. The existence of two competitive formation processes was suggested for the formation of goethite and hematite. Goethite is formed via solution, preferably from monovalent Fe(III), [$Fe(OH)_2^+$ and $Fe(OH)_4^-$], and hematite by internal rearrangement and dehydration within ferrihydrite aggregates. They stated that the conditions favourable for the formation of goethite are unfavourable for that of hematite and *vice versa* [66].

Yasuhiro et al. prepared submicrometer, crystalline hematite (α-Fe_2O_3) particles by hydrolysis of organic iron carboxylate solutions using water at 175ºC for 30 minutes [67]. The particle size of hematite was significantly dependent on the liquid-phase stirring speed and the organic compositions. The precipitation rate of hematite from the organic solution followed first-order kinetics. The precipitation rate increased markedly with increasing temperature and the activation energy for the process was 94.6 kJ/mol. At 220ºC, the hydrolysis of iron carboxylate solution leads to a mixture of hematite and magnetite (Fe_3O_4). The iron oxides prepared at 175ºC-220ºC were found to be free from organic contamination of the starting material. The precipitate of hematite was characterized by XRD), Infra-red and differential thermal analysis (DTA) and the particle size and morphology were obtained by using SEM [67].

Kandori et al. prepared hematite particles by forced hydrolysis reaction of acidic $FeCl_3$ solution and the effect of polyvinyl alcohol (PVA) on the formation of the spherical hematite particles was examined [68]. When the concentration of polyvinyl alcohol was increased, the shape of hematite particles varied from spherical to disk-like by reducing their thickness. The hematite particles formed with polyvinyl alcohol were hydrohematite with a crystal lattice distortion and exhibited a polycrystalline nature. These particles change from microporous to mesoporous after the elimination of residual polyvinyl alcohol molecules adsorbing on cluster particles by evacuating the samples above 300ºC. This result supports the fact that hematite particles produced by the forced hydrolysis reaction are aggregates, as were further revealed by using simultaneous temperature programmed desorption, mass spectroscopy and thermogravimetric measurement. They characterized synthetic hematite particles by using TEM, SEM, XRD, mass spectroscopy, and thermogravimetric analysis in vacuo. TEM and SEM were performed under acceleration voltages of 100 and 15KV with JEOL-200B and JSL-5600 instruments,

respectively. Adsorption experiment of polyvinyl alcohol (PVA) was measured at 25ºC and 90ºC using a TOC elemental analyzer. The TEM result shows that the change of particle size with the addition of PVA is little. The fraction of particles lost their spherical habit and acquired an ellipsoidal shape. The SEM result clarified that the spherical particles vary their shape to disk-like by reducing their thickness. Therefore, it can be defined that the disk-like but not ellipsoidal particles are produced in the presence of PVA. Also, from their TEM pictures it was seen that the particles produced with PVA are porous and possess a high surface area. All of the particles produced with PVA exhibited the characteristic x-ray diffraction pattern of hematite, (JCPDS 33-664), although the intensity of the patterns decreased with increasing PVA concentrations as the particles are polycrystalline and their crystallinity was reduced [68].

Gee et al. prepared hematite nanoparticles by forced hydrolysis of acidic Fe^{3+}. 0.02 mol of HCl was added to deionized water in a closed container and the temperature was increased until the water boiled. The temperature was kept constant at about 98ºC through thermal wraps. With a feedback temperature controller, 0.04 mol of $FeCl_3 \cdot 6H_2O$ was added under continuous stirring to obtain an Fe solution and was left in the container for 48 hours. The resulting red precipitate was separated from the solution by centrifugation and washed with deionized water to remove cations and anion at pH 7 [69]. The produced sample was dried at 80ºC for 6 hours in a drier oven and had a fairly uniform size of 40 nm. The powder sample was characterized using XRD, TEM, and Mossbauer spectroscopy. Nanostructured hematite can be prepared by electrochemical synthesis [70] by decomposition of organic iron compounds in alkaline media (pH >12) or by oxidation of pure iron at high temperature [71, 72].

Galvez et al. prepared synthetic hematite in the presence of phosphate that can incorporate phosphorus (P) in forms other than phosphate adsorbed by ligand-exchange on the crystal surface. Thirteen ferrihydrites with co-precipitated P were prepared by adding 1M KOH to 200 cm^3 of a continuously stirred 0.135 M $Fe(NO_3)_3$ solution containing KH_2PO_4 until the pH was 4 [73]. The resulting ferrihydrite suspension was centrifuged and 190 cm^3 of the supernatant was discarded. Solid $Mg(NO_3)_2 \cdot 6H_2O$ and water were added to make the Mg concentration 2M to prevent the formation of goethite. After readjusting the pH to 4, the suspension was poured into a pyrex bottle and placed in an oven at 373±1 K. Crystallization of the hematite was complete when the volume occupied by the initial gelatinous precipitate was reduced to less than one-tenth of the original and the color of the sediment was bright red. After cooling, centrifugation, and decantation, the sediment was washed with 0.5M HNO_3 to dissolve any residual ferrihydrite, twice with 0.1M KNO_3 at pH 3 and twice with 0.1M KOH-0.5M KNO_3 to remove phosphate adsorbed on the surface of hematite. The substituted hematite was characterized by determining the surface area and the micropore surface area using N_2 adsorption (BET and t-plot methods, respectively) with a micrometrics ASAP 2010 surface area analyzer.

Oxyanion Removal by Adsorption on Iron Oxides

Oxyanion

Oxyanion (or oxoanion) is a chemical compound with the generic formula $A_xO_y^{z-}$ (where A represents a chemical element and O represents an oxygen atom). Oxyanions are formed by a large majority of the chemical elements [74]. The formulae of simple oxyanions are determined by the octet rule. The structures of condensed oxyanions can be rationalized in terms of AO_n polyhedral units with sharing of corners or edges between polyhedra. There are different types of oxyanions: the monomeric and the poly meric. The formula of monomeric oxyanions, AO_n^{m-}, is dictated by the oxidation state of element A and its position in the periodic table. Elements of the first row are limited to a maximum coordination number of 4. However, none of the first row elements has a monomeric oxyanion with that coordination number. Carbonate (CO_3^{2-}) and nitrate (NO_3^-) have a trigonal planar structure with π bonding between the central atom and the oxygen atoms. This π bonding is favoured by the similarity in size of the central atom and oxygen.

The oxyanions of second-row elements in the group oxidation state are tetrahedral. Tetrahedral SiO_4 units are found in olivine minerals $(Mg,Fe)SiO_4$ but the anion does not have a separate existence as the oxygen atoms are surrounded tetrahedrally by cations in the solid state. Phosphate (PO_4^{3-}), sulphate (SO_4^{2-}), and perchlorate (ClO_4^-) ions can be found as such in various salts. Examples are borate (BO_3^{3-}), carbonate (CO_3^{2-}), nitrate (NO_3^-), phosphate (PO_4^{3-}), sulphate (SO_4^{2-}), chromate (CrO_4^{2-}), arsenate (AsO_4^{3-}), nitrite (NO_2^-), phosphite (PO_3^{3-}), sulphite (SO_3^{2-}), arsenite (AsO_3^{3-}), hypophosphite (PO_2^{3-}), hyposulfite (SO_2^{2-}), etc.

A polyoxyanion is a polymeric oxyanion in which multiple oxyanion monomers, usually regarded as MO_n polyhedra, are joined by sharing corners or edges [75] When two corners of a polyhedron are shared, the resulting structure may be a chain or a ring. Short chains occur, for example, in polyphosphates. Inosilicates, such as pyroxenes, have a long chain of SiO_4 tetrahedrals (each sharing two corners. The same structure occurs in meta-vanadates such as ammonium metavanadate (NH_4VO_3).

Examples of oxyanion contamination of groundwater include: perchlorate, borate, arsenate, selenate, chromate, and molybdate [76-79]. Other oxyanions found in ground water are nitrates, sulphates, carbonates, and phosphates.

Perchlorate salts are used in solid propellants (in rockets and missiles), munitions, commercial explosives, fireworks, and flares. Perchlorate compounds are also used in a number of other manufacturing operations (e.g. electroplating, pharmaceutical production, paints, and enamels) and agricultural uses [78, 80]. Perchlorate salts are highly soluble in water and the perchlorate anion has little affinity for most geologic materials except various oxides [80-82].

Removal of Oxyanion

The oxyanions of major concern today are arsenate, arsenite, chromate, phosphate, vanadate, and selenate. A few familiar methods in practice for the removal of these oxyanions are chemical precipitation, ion exchange, solvent extraction, reverse osmosis, and adsorption. Reverse osmosis, although very effective, is a cost-prohibitive process as membranes get easily spoiled, requiring frequent replacement. Chemical precipitation is not very suitable when the pollutants are present in trace amounts and sludge also is produced. Solvent extraction or electrolytic processes are also available, but they are considered to be cost-effective only for more concentrated solutions. Ion exchange is expensive and sophisticated. The process of adsorption has become one of the preferred methods for the removal of toxic contaminants from wastewater as it has been found to be very effective, economical, versatile, and simple [83]. Adsorption has the additional advantages of applicability at very low concentrations, suitability for using batch and continuous processes, ease of operation, little sludge generation, possibility of regeneration and re-use and low capital cost [84].

Adsorption of Some Oxyanions on Iron Oxides by Different Researchers

Gimenez et al. studied the sorption of As(III) and As (V) on different natural oxides (hematite, magnetite, and goethite) as a function of different parameters such as pH and adsorbate concentration. The sorption kinetics for the three iron oxides showed that equilibrium was reached in less than two (2) days and the kinetics of sorption was faster for goethite and magnetite than for hematite. The variation of the arsenic sorbed on the three different sorbents as a function of the equilibrium arsenic concentration in solution was fitted with a non-competitive Langmuir isotherm. The main trend observed in the variation of the arsenic sorbed with pH is a decrease of the sorption on the three sorbents at alkaline pH values. Highest As (III) sorption was observed on hematite surface in all the pH range compared to goethite and magnetite. Natural minerals studied in their work had similar sorption capacities for arsenic when compared with synthetic sorbents [85].

Ona-nguema et al. studied the modes of As (III) sorption onto two-line ferrihydrite, hematite, goethite, and lepidocrocite under anoxic conditions using XAS. X-ray absorption near edge structure spectrocopy (XANES) indicated that the absence of oxygen minimized As (III) oxidation due to Fenton reactions. Extended x-ray absorption fine structure spectroscopy (EXAFS) indicated that As (III) forms similar inner sphere surface complexes on two-line ferrihydrite and hematite that differ from those formed on goethite and lepidocrocite [86].

Fendorf et al. in their study observed that the molecular structure of ions retained on mineral surfaces is needed to accurately model their sorption process and to determine their stability. Extended x-ray absorption fine structure (EXAFS) spectroscopy was used in the study to deduce the local coordination environment of two environmental contaminants, arsenate and chromate on the mineral goethite (α-FeOOH). Based on the oxyanion-Fe distances, it was concluded that three different surface complexes exist on goethite for both oxyanions, a monodentate complex, a bidentate binuclear complex, and a bidentate- mononuclear complex. At low surface coverage, the bidentate complexes were more prevalent. They observed that the bidentate binuclear complex appears to be in the greatest proportion at the highest surface coverages [87].

Ding et al. also studied the adsorption of three anions (AsO^{3-}, PO_4^{3-}, and CrO_4^{2-}) and two cations (Zn^{2+} and Pb^{2+}) on a new form of armophous black ferric oxyhydroxide that resembles in local structure β-FeOOH, akaganeite. The nature of the interaction between FeOOH substrate and the adsorbates was characterized with x-ray photoelectron spectroscopy on the core and valence band levels of trivalent iron and oxygen using frontier molecular orbital theory as a theoretical framework. Their findings indicated that substantial and variable charge transfer occurs in which the FeOOH substrate can function either as a Lewis acid or base in its interaction with different adsorbates. It was also suggested that the valence band spectra can be used to estimate qualitatively the energy level separation between the highest occupied molecular orbital (HOMO) and lowest unoccupied molecular orbital (LUMO) of the surface complexes and to assess the chemical affinity between substrate and adsorbate [88].

Weerasooriya and Tobschall investigated the adsorption of CrO_4^{2-} onto goethite as a function of pH, background electrolyte, and adsorbate loading. Experimental data were interpreted with a three-plane model (TPM) that accounts for spatial charge distribution of inner sphere surface complexes. In their study, the influence of co-anions such as Cl^-, NO_3^-, PO_4^{3-}, and SO_4^{2-} and temperature were not considered. In accordance with EXAF spectroscopic data $>FeO^{0.2}\ CrO_3^{-1.3}$ and $> (FeO)_2^{0.4}\ CrO_2^{-0.6}$ surface species were selected for TPM calculations. TPM simulations replicate CrO_4^{2-} adsorption data well when CrO_4^{2-} coverage was $<2x\ 10^{-7}$ mol·m^{-2} [89].

Foster-Mills et al. studied the sorption of chromate and phosphate onto hematite surface. They studied the thermodynamics and kinetics of the sorption of Cr(VI), a contaminant found in ground water at many United States of America Department of Energy Nuclear Sites and industrial sites on powdered hematite (α-Fe_2O_3). Batch sorption experiments were performed to determine the maximum sorption capacities of Cr(VI), phosphate and sulphate oxyanion on hematite. Competitive sorption between Cr(VI), phosphate and sulphate oxyanions were examined using laser photoacoustic spectroscopy (LPAS) [90].

Smith and Ghiassi also studied chromate removal by an iron sorbent. In the study, a solution containing chromate was treated using waste shot-blast fines recovered from surface finishing operations in a cast-iron foundry as adsorbent in batch and fixed-bed modes. Equilibrium experiments for initial chromate concentration of 5 to 10

ppm produced a pH-adsorption edge that exhibited removal of chromium (Cr) over a broad pH range and with adsorption capacities that compared favourably to those reported for other adsorbents such as activated carbon and commercial iron oxides. Surface complexation modeling of adsorption equilibria suggested the formation of monodentate inner sphere complexes with chromate (CrO_4^{2-}) and bichromate ($HCrO_4^-$). Adsorption of Cr (VI) as iron-oxy-hydroxide sites appears to be the primary mechanism of chromium removal at neutral pH. At lower pH values (i.e. pH 4), reduction to Cr(III) is assumed to contribute to the increasing removal as a function of decrease in pH [91].

Peacock and Sherman studied the adsorption of V(V) onto goethite (α-FeOOH) under oxic (ρ_{02} = 0.2bar) atmospheric conditions. EXAFS spectra showed that V(V) adsorbs by forming inner sphere complexes as $VO_2(OH)_2$ and $VO_3(OH)$. They predicted the relative energies and geometries of $VO_2(O,OH)_2$-FeOOH surface complexes using ab-initio calculations of the geometries and energetics of analogue $Fe_2(OH)_2(H_2O)_6$ $O_2VO_2(O,OH)_2$ clusters. The bidentate corner-sharing complex was predicted to be substantially (57 kJ/mol) favored energetically over the hypothetical edge-sharing bidentate complex. Fitting the EXAFS spectra using multiple scattering showed that the only bidentate corner-sharing complex was present with Fe-V and V-O distances in good agreement with those predicted. They found it important to include multiple scatterings in the fits of their EXAFS data otherwise spurious V-Fe distances near 2.8 Å, which may be incorrectly attributed to edge-sharing complexes. No evidence for monodentate complexes was found, which agrees with predicted high energies of such complexes. Having identified the $FeO_2V(OH)_2^+$ and $Fe_2O_2VO(OH)^0$ surface complexes, they were able to fit the experimental vanadium (V) adsorption data to the reaction [92]:

$$2FeOH_2^+ + VO_2^+ \leftrightarrows Fe_2O_2(OH)_2^+ + 2H^+ \quad (6)$$

and

$$2FeOH + HVO_4^{2-} \leftrightarrows Fe_2O_2VO(OH)^0 + 2OH^- \quad (7)$$

The dissociation constant of the $Fe_2O_2VO_2H_2^+$ surface complex was also determined.

Naeem et al. summarized known vanadium occurrence in North American group water and assessed vanadium removal by three commercially available metal oxide adsorbents with different minerologies. Preliminary vanadate adsorption kinetics onto GFH, E-33, and GTO had been studied and the homogeneous surface diffusion model (HSDM) was used to describe the adsorption kinetic data. The effects of pH, vanadium concentration, and volume/mass ratio were assessed. Vanadium adsorption decreases with increasing pH, with maximum adsorption capacities achieved at pH 3-4. Results indicated that all adsorbents removed vanadium, and that GFH has the highest adsorption capacity, followed by GTO and E-33. Data were best fitted with the Langmuir model rather than Freundlich isotherm. Both sorption maxima (Xm) and binding energy constant (b) followed the trend GFH> GTO> E-33. Naturally occurring vanadium was also removed from Arizona ground water in rapid small-scale column tests (RSSCT') [93].

O'Reilly et al. observed that sorption was initially rapid, with over 93% arsenate being sorbed in a 24-hr period at pH 6 onto goethite. Similar arsenate adsorption behavior was observed at pH 4. Analysis of the sample with extended x-ray absorption fine atomic shells surrounding the adsorbed As. The closest shell was identified as an O atom, the next shell out was identified as an Fe atom. The As-Fe bond distance of 3.30 Å, derived from XAFS data was indicative of a bidentate binuclear bond forming between the arsenate atoms and goethite surface. Their result was in agreement with the findings of previous researchers. Analysis of the As EXAFS from samples incubated for various periods indicated that the molecular environment did not change over time. Complimentary desorption kinetics studies showed that when aging was increased, there was no significant change in the amount of arsenate desorbed from geothite by PO_4^{3-} [94].

Researchers have shown that arsenate is specifically sorbed onto iron oxides such as goethite through an inner-sphere complex via a ligand exchange mechanism [87, 95, 96]. They found that using transmission-fourier transform infrared (T-FTIR) and attenuated total reflectance FTIR (ATR-FTIR) spectroscopy, arsenate replaced two singly coordinated surface OH groups to form binuclear bridging complexes.

Lumsdon et al. utilized infrared spectroscopy to discover that $HASO_4^{2-}$ ion participitated in ligand exchange reactions displacing singly coordinated surface hydroxyl groups to adsorb as a binuclear species [95]. EXAFS studies by Fendorf [87], Waychunas et al. [97], and Manceau [98] found that bidentate binuclear complexation was the major bonding mechanism for arsenate adsorption on goethite. On the basis of pressure jump relaxation study and EXAFS, it was demonstrated that arsenate can form three types of surface complexes on goethite, depending on the surface coverage [87, 96].

The list of some oxyanions investigated for their adsorption characteristics with various iron oxides are shown in Table 3.

Adsorption Isotherms and Adsorption Capacities

Adsorption isotherm describes how adsorbates interact with adsorbents, and this information is essential in optimizing the use of adsorbent. Table 4 summarizes some literature values on adsorption capacities of various oxyanions on different iron oxides. The affinities of iron oxides for oxy-anion can generally be grouped into the ranges: 2.35×10^{-5} mol/g-0.607 mmol/g for (U(VI)); 3.13 μmol/g-6.0 mg/g for chromate (Cr(VI)); 0.69 to 9.4 mg/g for arsenite (As(III)); and 39.8 μmol/g-70.4 mg/g for arsenate (As(V)) on the various iron oxides. The adsorption isotherms employed include Langmuir, Freundlich, and Dubinin Radushkevich. For most of the adsorption data of

Table 3. Some oxyanions investigated for their adsorption characteristics with various iron oxides.

Oxyanion	Types of Iron oxide	Reference
Arsenate	Ferrihydrite	Carbante et al. 2009 [99]
Phosphate	Ferrihydrite and goethite	Borggaard et al. 2005 [100]
Arsenate	Granular ferric hydroxide	Streat et al. 2008 [101]
Arsenite and Arsenate	Magnetite	Simeonidis et al. 2011 [102]
Chromate Cr(VI)	Magnetite	Namdeoand Bajpai, 2008 [103]
Chromate Cr(VI)	Hematite and Goethite	Ajouyed et al. 2010 [104]
Chromate Cr(VI)	Hematite	Singh at al, 1993 [105]
Chromate Cr(VI)	Chitosan-Magnetite nanocomposite	Bajpai and Armo, 2009[106]
U (VI	Hematite	Zhao at al, 2012 [107]
Uranyl	Hematite	Lefevre et al. 2006 [108]
Arsenate	Iron oxide impregnated Activated Carbon	Vaughan and Reed, 2005 [109]
Cr(VI)	Magnetite	Kendelewicz et al. 2000 [110]
Arsenite and Arsenate	Goethite and Armophous iron hydroxide	Lenoble et al. 2002 [111]
Phosphate and Arsenate	Goethite	Gao and Mucci, 2003[112]
Arsenate	Hematite, goethite, lepidocrocite, ferrihydrite	Sherman and Randall, 2003 [113]
Arsenate	Akaganeite	Deliyanni et al. 2003 [114]
Selenite and Selenate	Goethite and hematite	Duc et al. 2003 [115]
Arsenate and Chromate	Schwertmannite	Regenspurg and Peiffer, 2005 [116]
Arsenate	Goethite	Lakshmipathiraj et al. 2006 [117]
Arsenite and Arsenate	Mn-substituted iron oxyhydroxide ($Mn_{0.13}Fe_{0.87}OOH$)	Lakshmipathiraj et al. 2006 [118]
Arsenate	Ferrihydrite	Jia et al. 2007 [119]
Phosphate and Arsenate	Goethite	Luengo et al. 2007 [120]
Arsenate	Iron oxide-based sorbent	Zeng et al. 2008 [121]
Chromate	Hematite	Yin and Ellis, 2009[122]
Arsenate	Hematite and goethite	Mamindy-Pajany et al. 2009 [123]
Arsenate and Arsenite	Ferrihydrite, feroxyhyte, goethite and hematite	Muller et al. 2010 [124]
U(VI)	Goethite	Yusan and Erenturk, 2011 [125]
Arsenate	Hematite, goethite, magnetite and zero valent iron	Mamindy-Pajany et al. 2011 [126]
Arsenite and Arsenate	Ferrihydrite	Zhu et al. 2011 [127]
Arsenite and Arsenate	Magnetite and hematite	Luther et al. 2011[128]

oxyanions on iron oxides, the Langmuir isotherm best describe adsorption data followed by the Freundlich isotherm and Dubinin Radushkevich, in that order.

The surface complexation model used on some of the adsorption data include the constant capacitance model and these are illustrated in Table 5. It is evident from the tables that the level of interaction of oxyanions with iron oxides is strongly influenced by the method of preparation, surface area, and pH.

Conclusions

The particle sizes of the synthesized iron oxides depend on the method of synthesis, with sizes ranging from 17 nm to 7.4 micrometers. Acid hydrolysis of iron (II) and iron (III) nitrate, chloride, and sulphate is a common method of synthesis for the various iron oxides, but with modification by different authors. The pH of solution influences the product formation and particle size is also dependent on

Table 4. Adsorption characteristics of various oxyanions with iron oxides.

Oxyanion	Iron oxide	Synthesis Method	Characterization Method	Surface Area (m^2/g)	Adsorption Capacity		Temp. K	Optimal pH	Kinetic Model	References
					L	F				
					mol/g $\times 10^{-5}$					
U(VI)	Hematite	Sol gel	FTIR XRD BET	398.5	2.35 2.51 2.76	6.14 5.87 4.65	298 318 338	<6		Zhao et al. 2012 [107].
U(VI)	Goethite	Hydrolysis	XRD, SEM, BET	37.29	0.607	0.053	298	5		Yusan and Erenturk, 2011 [125]
					mg/g					
Cr (VI)	Hematite Goethite	Commercial	BET	1.7 11.6	2.299 1.955	0.544 0.348	298 298	≤ 5 ≤ 3		Ajouyed et al. 2010 [104].
					mg/g					
Cr(VI)	Magnetite	Precipitation	FTIR XRD TEM		1.5260 3.0693 3.9572		303 313 323			Namdeo and Bajpai, 2008 [103].
Cr(VI)	Hematite	Natural	BET		3.13 µmol/g	0.087	313			Singh et al, 1993 [104].
Cr(VI)	Chitosan-magnetite nanocomposite	Precipitation	FTIR, TEM TGA		1.515 1.266 1.006					Bajpai and Armo, 2009 [106].
					mg/g					
Arsenate Arsenite	Mn-FeOOH	Oxidation	XRD, FTIR BET	101	5.72 4.58			6-7		Lakshmipathiraj,2006 [118].
Arsenate	Ce (VI) doped iron oxide	Precipitation	FTIR, BET		70.4 mg/g		293	5.0	Pseudo first order	Zhang et al, 2003 [129]
					mmol/g					
Arsenate	Akaganeite	Precipitation	XRD, FT-IR, SEM	330	1.79 2.24 2.89	2.4 3.6 5.2	298 308 318	7.5		Deliyanni et al, 2003 [114].
Arsenate	Ferrihydrite	Hydrolysis	XRD, FT-IR				348	3		Jia et al, 2007 [119].

Table 4. Continued.

Oxyanion	Iron oxide	Synthesis Method	Characterization Method	Surface Area (m^2/g)	Adsorption Capacity		Temp. K	Optimal pH	Kinetic Model	References
					L	F				
Arsenate Arsenite	Goethite	Hydrolysis	XRD FTIR BET DTA/TGA	39				<4 4<pH<9		Lenoble et al. 2002 [111]
Arsenate	Goethite	Oxidation	FTIR, BET	103	1941 mol^{-1}		302	5.0		Lakshmipathiraj,2006 [117]
Arsenite	Iron oxide coated cement	Precipitation	XRD, EDX, PZC		0.69	0.22	300		Pseudo second order	Kundu and Gupta, 2007 [131]
Arsenate	Iron hydroxide based sorbent	Commercial	XRD, XRF, XPS, BET	236	22.2		293			Zeng et al, 2008 [121]
Arsenate Arsenite Cr(VI)	Magnetite Maghemite Nanoparticles	Commercial	BET, SEM, XPS	49	10.6 9.4 6.0		298	5 5 4.5		Chowdhury and Yanful, 2010 [132]
Arsenate	Goethite oil-coated Goethite	Hydrolysis	XRD, BET, FT-IR	35.4 9.3	97.1 µmol/g 39.8 µmol/g		298	4 4	Pseudo first and second order and	Wainipee et al, 2010 [133]

L – langmuir adsorption isotherm, F – freundlich adsorption isotherm, BET – brunnauer emmett teller, XRD – X-ray diffraction, FT-IR – fourier transform infra red, SEM – scanning electron microscopy, TEM – Transmission Electron Microscopy, TGA – Thermogravimetric Analysis, DTA – differential thermogravimetric analysis, ATR-FTIR – attenuated transmittance reflectance – fourier transform infrared, EDX – energy dispersive X-ray, PZC – point of zero charge, XPS – X-ray photoelectron spectroscopy

Table 5. Surface complexation modeling of oxyanions on iron oxides.

Oxyanion	Iron oxide	Synthesis Method	Characterization Method	Surface Area (m^2/g)	Adsorption Modeling	Temp. K	Optimal pH	Kinetic Model	References
Arsenate	Hematite Goethite	Commercial	BET, PZC	1.66 11.61	Inner-sphere complexation		7.0		Mamindy-Pajany et al, 2009 [123]
Selenate Selenite	Goethite and Hematite	Commercial powder	BET	20 8.4	Constance Capacitance model				Duc et al, 2003[115]
Vanadate	Goethite	Hydrolysis	XRD, BET	32.73	Inner sphere complexation				Peacock and Sherman, 2004 [92]
Phosphate Arsenate in seawater	Goethite	Hydrolysis	XRD, BET	33.5	CCM		<6.5 >7.0		Gao and Mucci, 2003 [112]
Arsenate	Ferrihydrite		XRD, BET, ATR-FTIR SEM		Bidentate Inner Sphere complex				Carabante et al 2009 [99]

stirring speed, and organic composition. The methods of synthesis also affect the points of zero charge of the iron oxides according to Marek Kosmulski PZC compilation.

Sorptive interactions between oxyanions and mineral surface have received considerable attention due to their important nutrient and contaminant roles and the ubiquitous distribution of minerals in aquatic, sedimentary, and terrestrial environments. Mineral surfaces, particularly metal (hydr) oxides, concentrate oxyanions through both specific and non-specific complexation mechanisms. Specifically adsorbed oxyanions are strongly surface associated through covalent bonds formed by ligand exchange with surface hydroxyl groups (inner-sphere complexed), whereas non-specifically adsorbed oxyanions are weakly surface associated due to electrostatic interaction through an intervening water molecule (outer-sphere complexed). It is therefore evident that further research needs to be carried out so as to have a better understanding of the mechanism of sorption of oxyanions on iron oxides. More efforts also need to be directed at defining optimal conditions for oxyanion removal from aqueous solution in column experiments and for ultimate industrial application.

Acknowledgements

Adegoke H. I. would like to thank the University of Ilorin for provision of the staff development award and the Cape Peninsula University of Technology (CPUT), Cape Town, South Africa, for a three-month research fellowship.

References

1. SCHWERTMANN U., AND CORNELL R.M Iron oxide in the laboratory: preparation and characterization. Wiley-VCH Weinheim, Germany, pp. 1-132, **1991**.
2. CORNELL R.M., SCHWERTMANN U. The iron oxides: structures, properties, reactions, occurrences and uses. Wiley VCH, **2003**.
3. TEJA A.S., KOH P.Y. Prog crystal Growth Charact. Mater. **55**, 22, **2009**.
4. MAHMOUDI M., SIMCHI S., IMANI M. Recent advances in surface engineering of superparamagnetic iron oxide nanoparticles for biomedical application J. Iran Chem. Soc. **7**, S1, **2010**.
5. WANG G., LIU T., LUO Y., ZHAO Y., REN Z., BAI J., WANG H. Preparation of Fe_2O_3/graphene composite and its electrochemical performance as an anode material for lithium ion batteries. J. Alloy. Compd. **2011**.
6. SINGH J., SRIVASTAVA M., DUTTA J., DUTTA P.K. Preparation and properties of hybrid monodispersed magnetic α-Fe_2O_3 based chitosan nanocomposite film for industrial and biomedical applications. Int. J. Biol. Macromol. **48**, 170, **2011**.
7. HASSAN M.F., GUO Z., CHEN Z., LIU H. α-Fe_2O_3 as an anode material with capacity rise and high rate capability for lithium-ion batteries. Mater. Res. Bull. **46**, 858, **2011**.
8. GUPTA A. K., GUPTA M. Synthesis and Surface engineering of iron oxide nanoparticles for biomedical applications. Biomaterials **26**, (18), 3995, **2005**.

9. MIMURA N., TAKAHARA I.,SAITO M., HATTORI T., OKHUMA K., ANDO M. Dehydrogenation of ethylbenzene over iron oxide-based catalyst in the presence of carbon dioxide. Catal. Today **45**, 61, **1998**.
10. CHANG J., PARK S., PARK M. Chem. Lett **11**, 1123, **1997**. In: WANG X., CHEN X., MA X., ZHENG H., JI M. ZHANG Z. Low-temperature synthesis of α-Fe_2O_3 nanoparticles with a closed cage structure. Chem. Phys. Lett. **384**, 391, **2004**.
11. TURNER J., HENDEWERK M., PARMETER J., NEIMAN D., SOMORJAL G. J. Electrochem. Soc. **131**, 177, **1984**. In: WANG X., CHEN X., MA X., ZHENG H., JI M. ZHANG Z. Low-temperature synthesis of α-Fe_2O_3 nanoparticles with a closed cage structure. Chem. Phys. Lett **384**, 391, **2004**.
12. LINDGREN L., WANG H., BEERMANN N., VAYSSIERES L., HAGFELDT A., LINGUIST S. Sol. Energ. Mat. Sol. C. **71**, 231, **2002**.
13. PENG X., QIAN X., MAO H., WANG A. Y., CHEN Z., NIE S., SHIN D. M. Targeted magnetic iron oxide nanoparticles for tumor imaging and therapy. Int. J. Nanomedicine. **3**, (3), 311, **2008**.
14. YU M., PARK J., JEONG Y. Y., MOON W. K., JON S. Integrin-targeting thermally cross-linked superparamagnetic iron oxide nanoparticles for combined cancer imaging and drug delivery. Nanotechnology **21**, (41), **2010**.
15. GHOSE S.K., PETITTO S.C, TANWAR K.S., LO C. S., ENG P.J., CHAKA A. M. TRAINOR T. P. Surface Structure and Reactivity of Iron oxides-Water interfaces. Dev. In Earth and Environ. Sciences. **7**, **2008**.
16. SORESCU M., MIHAILA-TARABASANU D., DIAMONDESCU L. Mossbauer and Magnetic study of substituted Magnetites. Appl. Phys. Lett. **72**, 2047, **1998**.
17. SYLVA R. M. The hydrolysis of Iron (III) Rev. Pure Appl. Chem. **22**, 115, **1972**.
18. MATIJEVIC E., SCHEINER P. Ferric hydrous Oxide sols. III Preparation of Uniform particles by hydrolysis of Fe (III) chloride-nitrate and perchlorate solutions. J. Colloid Interface Sci. **63**, 509, **1978**.
19. OZAKI, M. KRATHVIL S., MATIJEVIC E. Formation of monodispersed spindle type hematite particles. J. Colloid interface Sci. **102**, 146, **1984**.
20. RAMMING T.P., WINNUBST A.J.A., VAN KATS C.M., PHILPSE A. P. The Synthesis and magnetic Properties of Nanosized Hematite (α-Fe_2O_3) particles. J. Colloid Interf. Sci. **249**, 346, **2002**.
21. QIN W., YANG C., YI R., GAO G. Hydrothermal Synthesis and Characterization of Single-Crystalline α-Fe_2O_3 Nanocubes. J. Nanomaterials **2011**.
22. FEITKNECHT W., MICHAELIS W. On the hydrolysis of Iron (III) perchlorate solution Chem. Acta **45**, 212, **1962**.
23. SCHWERTMAN U, FISCHER W. R. The preparation of α-FeOOH and α-Fe_2O_3 from amorphous iron (III) hydroxide. J. of Inorganic and General Chemistry. **346**, 137, **1966**.
24. CORNELL R. M., GIOVANOLI R., SCHINEIDER W. Review of the hydrolysis of iron (III) and the crystallization of amorphous iron (III) hydroxide hydrate. J. Chem. Technol. Biotechnol. **46**, 115, **1989**.
25. SCHWERTMANN U., MURAD E. Effect of pH on the formation of goethite and hematite from ferrihydrite. Clay. Clay Miner. **31**, 277, **1983**.
26. FEITKNECHT W. On the oxidation of hydroxyl compounds of iron in aqueous solutions. J. Electrochem. **63**, 34, **1959**.
27. SCHWERTMAN U. The synthesis of defined iron oxides under different conditions. J. of Inorganic and General Chem. **298**, 337, **1959**.
28. HIEMSTRA T., DE WIT J. C. M., VAN RIEMSDIJK W.H. Multisite Proton Adsorption Modeling at the solid/solution Interface of Hydr(oxides): A New Approach. J. Colloid and Interface Sci. **133**, (1) 91, **1989**.
29. MACKAY A. L. Some aspects of the topochemistry of the iron oxides and hydroxide. In: J. H. de Boer (Ed.) Reactivity of Solids. Proc. 4th Intern. Symposium on reactivity of solids, 571, **1961**.
30. SAPIESKO R. S., MATIJEVIC E. Preparation of well-defined colloidal particles of thermal decomposition of metal chelates. I. Iron oxides. J. colloid interface Sci. **74**, 405, **1980**.
31. DUHAN S., DEVI S. Synthesis and Structural characterizationof Iron oxide-silica nanoparticles Prepared by the solgel method. Int. j of Electronics Eng. **2**, (1), 89, **2010**.
32. GONG C., CHEN D., JIAO X. WANG Q. Continuous hollow α-Fe_2O_3 and α-Fe fibers prepared by sol-gel method, J. of Materials Chemistry **12**, (6), 1844, **2002**.
33. HOLLAND H., YAMAURA M. Synthesis of Magnetite Nanoparticles by microwave irradiation and characterization. Seventh Internat. Latin American Conference on Powder technol. (PTECH) **2009**.
34. PARSONS J.G., LUNA C., BOTEZ C.E., ELIZALDE J., GARDEA-TORRESDEY J.L. Microwave-assisted synthesis of iron (III) oxyhydroxides/oxides characterized using transmission electron microscopy, X-ray diffraction and X-ray absorption spectroscopy. J. Phys. Chem. Solids **70**, 555, **2009**.
35. NI Y., GE X., ZHANG Z., YE Q. Fabrication and Characterization of plate-shaped γ-Fe_2O_3 nanocrystals. Chemistry of Materials **14**, (3), 1048, **2002**.
36. WILSON M.J. A handbook of determinative methods in clay mineralogy. Blakie, Glasgow and London pp. 308, **1987**.
37. KOSMULSKI M., MACZKA E., JARTYCH E. ROSENHOLM J.B. Synthesis and characterization of goethite and goethite-hematite composite: experimental study and literature survey. Adv. Colloid and Interface Sci. **103**, 57, **2003**.
38. GRAFE M., EICK M.J, GROSS P.R. Adsorption of Arsenate and Arsenite on Goethite in the presence and absence dissolved carbon dioxide. Soil Sci. Am. J. **65**, 1680, **2001**.
39. MORAIS F. I., PAGE A. L., LUND L. J. The Effect of pH Salt Concentration and Nature of Electrolytes on the Charge Characteristics of Brazilian Tropical Soils. Soil Sci, Soc. Am. J. **40**, 521, **1976**.
40. PARKS G. A., DE BRUYN P. L. The Zero Point of Charge of Oxides. J. Phys. Chem. **66**, 967, **1961**.
41. BOURIKAS K., KORDULIS C., LYCOUGHIOTIS A. Differential Potentiometric Titration: Development of a Methodology for determining the point of zero charge of metal (hydr)oxides by one Titration curve. Environ. Sci. Technol. **39**, 4100, **2005**.
42. KOSMULSKI M. The pH-dependent surface charging and the points of zero charge. J. Colloid Interf. Sci. **253**, 77, **2002**.
43. KOSMULSKI M. pH-Dependent Surface Charging and Points of Zero charge III. Update. J. Colloid Interf. Sci. **1**, (50), 1, **2006**.
44. PAN P. Z., SOMASUNDARAN P., TURRO N. J. JOCKUSCH S. Interactions of cationic dendrimers with hematite mineral. Colloid. Surfface. A **238**, 123, **2004**.

45. KIRWAN L. J., FAWELL P. D., VAN BRONSWIJK W. An *in-situ* FTIT-ATR study of polyacrylate adsorbed onto hematite at high pH and high ionic strength Langmuir **20**, 4093, **2004**.
46. DAS M. R., BORDOLOI D., BORTHAKUR P. C., MAHI-UDDIN S. Kinetics and adsorption of benzoate and saliylate at the natural-water interface. Colloid. Surface A **254**, 49, **2004**.
47. ADDAI MENSAH J., RALSTON J. Interfacial chemistry and particle interactions and their impact upon the dewatering behaviour of iron oxide dispersions. Hydrometallurgy **74**, (3-4), 221, **2004**.
48. PEACOCK C.L., SHERMAN D. M. Copper(II) sorption onto goethite, hematite and lepidocrocite: a surface complexation model based on ab initio molecular geometries and EXAFS spectroscopy Geochim Cosmochim Acta **68**, 2623, **2004**.
49. CHIBOWSKI S., PATKOWSKI J. OPALA-MAZUR E. Adsorption of Commercial, Filtrated and Fractionated Polyethylene Oxide on Hematite Mater. Chem. Phys. **92**, 519, **2005**.
50. JARLBRING M., GUNNERIUSSON L., HUSSMANN B. FORSLING W. Surface complex characteristics of synthetic maghemite and hematite in aqueous suspensions J. Colloid Interf. Sci. **285**, 212, **2005**.
51. FAN M., BOONFUENG T., XU Y., AXE L., TYSON T. A. Modeling Pb Sorption to Microporous Amorphous Oxides as Discrete Particles and Coatings J. Colloid Interf. Sci. **281**, 39, **2005**.
52. KRELLER D. I., GIBSON G., VAN LOON G.W. HORTON J.H. Chemical force microscopy investigation of phosphate adsorption on the surfaces of hydrous ferric oxide particles J. Colloid Interf. Sci. **254**, 205, **2002**.
53. DAVRANCHE M., POURRET O., GRUAU G., DIA A. Impact of humate complexation on the adsorption of REE onto Fe oxyhydroxide. J. Colloid Interf. Sci. **277**, 271, **2004**.
54. PEACOCK C. L., SHERMAN D.M. Copper(II) sorption onto goethite, hematite and lepidocrocite: a surface complexation model based on ab initio molecular geometries and EXAFS spectroscopy. Geochim. Cosmochim. Ac. **68**, 1723, **2004**.
55. SAITO T., KOOPAL L. K., VAN RIEMSDIJK W.H, NAGASAKI S., TANAKA S. Adsorption of humic acid on goethite: Isotherms, charge adjustments, and potential profiles. Langmuir **20**, 689, **2004**.
56. VARANDA L.C., MORALES M. P., GOYA G. F., IMAIZUMI M., SERNA C.J., JAFELICCI M. Magnetic properties of acicular Fe1-xREx (RE = Nd, Sm, Eu, Tb; x = 0, 0.05, 0.10) metallic nanoparticles. Mater. Sci. Eng. B **112**, 188, **2004**.
57. BOILY J. F., SJOBERG S., PERSSON P. Structures and Stabilities of Cd(II) and Cd(II)-Phthalate Complexes at the Goethite/Water Interface. Geochim. Cosmochim. Ac. **69**, 3219, **2005**.
58. JUANG R.S., CHUNG J.Y. Equilibrium sorption of heavy metals and phosphate from single- and binary-sorbate solutions on goethite. J. Colloid Interf. Sci. **275**, 53, b.
59. XU Y., AXE L. Synthesis and Characterization of Iron Oxide-Coated Silica and Its Effect on Metal Adsorption. J. Colloid Interf. Sci. **282**, 11, **2005**.
60. ANTELO J., ARENA A., FIOL S., LOPEZ R. ARCE F. Effects of pH and ionic strength on the adsorption of phosphate and arsenate at the goethite-water interface J. Colloid Interf. Sci. **285**, 476, **2005**.
61. NIELSON U. G., PAIK Y., JULMIS K., SCHOONEN M. A. A., REEDER R.J. GREY C. Investigating Sorption on Iron-Oxyhydroxide Soil Minerals by Solid-State NMR Spectroscopy: A 6Li MAS NMR Study of Adsorption and Absorption on Goethite J. Phys. Chem. B. **109**, 310, **2005**.
62. WANG X., CHEN X., MA X., ZHENG H., JI M. ZHANG Z. Low-temperature synthesis of α-Fe_2O_3 nanoparticles with a closed cage structure. Chem. Phys. Lett. **384**, 391, **2004**.
63. YU W., HUI L. Preparation of Nano-needle Hematite particles in solution. Mat. Res. Bull. **34**, (8) 1227, **1999**.
64. LI Y., LIAO H., QIAN Y. Hydrothermal synthesis of ultrafine α Fe_2O_3 and Fe304 powders Mat. Res. Bull. **33**, (6), 841, **1998**.
65. SORESCU M., BRAND R.A, MIHAILA- TARABASANU D., DIAMANDESCU L. Synthesis and magnetic properties of hematite with different particle morphologies. J. Alloy. Compd. **280**, 273, **1998**.
66. SCHWERTMANN U., MURAD E. Effect of pH on the formation of goethite and hematite from ferrihydrite. Clay. Clay. Miner. **31**, 277, **1983**.
67. YASUHIRO K., TAKESHI K. SATORU A. Preparation and Properties of fine hematite powders by hydrolysis of iron carboxylate solutions. Metall. Mater. Trans. B, **25**, (2) 165, **1994**.
68. KANDORI K., YAMAMOTO N., YASUKAWA A. ISHIKAWA T. Preparation and characterization of disk-shaped hematite particles by a forced hydrolysis reaction in the presence of polyvinyl alcohol Phys. Chem. Chem. Phys **4**, 6116, **2002**.
69. GEE S. H., HONG Y. K, SUR J. C., ERICKSON D. W., PARK M. H. JEFFERS F. Spin orientation of hematite (α-Fe_2O_3) nanoparticles during the Morin transition. IEEE Transaction on magnetic **40**, (4), **2004**.
70. PASCAL C., PASCAL J., FAVIER F., ELIDRISSI M., PAYEN C. Electrochemical synthesis for the control of γ-Fe_2O_3 nanoparticle size.Morphology, microstructure and magnetic behaviour. Chem. Mater. **11**, 144, **1999**.
71. FU Y., CHEN J., ZHANG H. Phys. Lett. 350, 491, 2001.In: ZHANG X., HAN Q., DONG Z., XU Y., ZHANG H. Thermal stability of Fe_2O_3 Nanowires. J. Mater Sci. **24**, (4), 1, **2008**.
72. FU Y., WANG R., XU J., CHEN J., YUN Y. NARLIKAN A., ZHANG H. 'Chem. Phys.Lett. **379**, 373, **2003**. In: ZHANG X., HAN Q., DONG Z., XU Y., ZHANG H. Thermal stability of Fe_2O_3 Nanowires. J. Mater Sci. **24**, (4), 1, **2008**.
73. GALVEZ N., BARRON V., TORRENT J. Preparation and properties of hematite with structural phosphorus. Clays and Clays Mineral **47**, (3), 375, **1999**.
74. GREENWOOD N., EARNSHAW A., Chemistry of the Elements 2nd ed.; Oxford: Butterworth-Heinemann, **1997**.
75. MUELLER U. Inorganic Structural Chemistry. **1993**.
76. PULS R. W., PAU L, POWELL R.M. The application of in-situ permeable reactive (zero-valent iron) barrier technology for the remediation of chromate-contaminated ground water: a field test. Appl. Geochim. **14**, (8), 989, **1999**.
77. EPA Proven treatment alternatives for above ground treatment of arsenic in ground water. Engineering Forum Issues Paper, EPA 542-S-02-002. U.S Environmental Protection Agency, Washington, DC **2002**.
78. EPA Perchlorate treatment technology update, Federal Facilities Forum Issue Paper, EPA 542 R-05-015. U.S Environmental Protection Agency, Washington, DC. http://www.epa.gov.sweri 01/download/remed/542-R-05-015.pdf **2005**.

79. DOHERTY R., PHILIPS D. H., MCGEOUGH K.L., WALSH K.P., KALIN R. M. Development of modified fly-ash as a permeable reactive barrier medium for a former manufactured gas plant site. Northern Ireland. Environ. Geol. **50**, (1), 37, **2006**.
80. ITRC Perchlorate: Overview of issues, status and remedial options. Interstate Technology and Regulatory Council, Washington, DC. http://www.epa.gov. sweti)1/download/remed/542-R-05-015.pdf **2005**.
81. MOTZER W.E. Perchlorate: problems, detection and solutions. Environ. Forensics **2**, (4), 301, **2001**.
82. URBANSKY E.T., BROWN S. K. Perchlorate retention and mobility in soils. J. Environ. Monitor. **5**, 455, **2003**.
83. TRAN H.H., RODDICK F.A., O'DONNELL J. A. Comparison of chromatography and dessicant silica gels for the adsorption of metal ions- I. Adsorption and kinetics. Water Res. **33**, 2992, **1999**.
84. MOHANTY K., DAS D., BISWAS M.N. Preparation and characterization of activated carbon from Steculia alata nut-shell by chemical activation with zinc chloride to remove phenol from waste water. Adsorption **12**, 119, **2006**.
85. GIMENENZ J., MARTINEZ M., PAPLO J., ROVIRA M., DURO L. Arsenic sorption onto natural hematite. Magnetite and goethite. J. Hazard. Mater. **141**, (3), 575, **2007**.
86. ONA-NGUEMA G., MORIN G., JUILLOT F., CALAS G., BROWN JR G.E. EXAFS Analysis of Arsenite Adsorption onto Two-line Ferrihydrite, Hematite, Goethite and Lepidocrocite. Environ. Sci. Techol. **39**, 9147, **2005**.
87. FENDORF S., EICK M.J, SPARKS D.L. Arsenate and chromate Retention mechanisms on Goethite I. Surface structure. Environ Sci. Technol **32**, (2), 315, **1997**.
88. DING M., DE JONG , B.H. W.S, ROOSENDAAL S.J., VREDENBERG A. XPS studies on the electronic structure of bonding between solid and solutes: adsorption of arsenate, chromate, Pb^{2+} and Zn^{2+} ions on amorphous black ferric oxyhydroxide. Geochim cosmochim. Acta. **64**, (7), 1209, **2007**.
89. WEERASOORIYA R., TOBSCHALL H.J. Mechanistic modeling of chromate adsorption onto goethite. Colloid. Surface A **162**, (1-3), 167, **2000**.
90. FOSTER-MILLS N.S, AMONETTE J.E, WILLIAM B.K., TAYLOR A.E. Competitive-Trace-level sorption of chromate and phosphate to Hematite surfaces: A spectroscopic Approach. Environ. Dynamic and simulation Annual report pp. 4, **1999**.
91. SMITH E., GHIASSI K. Chromate removal by an iron sorbent: mechanism and modeling. Water Environ. Res **78**, (1), 84, **2006**.
92. PEACOCK L. C., SHERMAN D. M. VANADIUM (V) Adsorption onto goethite (α-FeOOH) at pH 1.5 to 12: A Surface Complexation model based on ab initio molecular geometries and EXAFS Spectroscopy. Geochim. Cosmochim. Ac. **68**, (81), 1723, **2004**.
93. NAEEM A., WESTERHOFF P., MUSTAPHA S. Vanadium Removal by Metal (hydr) oxide Adsorbents. Water Res. **41**, 5196, **2007**.
94. O'REILLY S. E., STRAWN D. G., SPARKS D. L. Residence Time Effects on Arsenate Adsorption/Desorption Mechanisms on Goethite. Soil Sci. Soc. Am. J. **65**, 67, **2001**.
95. LUMSDON D. G., FRASER A.R., RUSSELL J.D., LIVESEY N.T. New Infrared band assignments for the arsenate ion adsorbed on synthetic goethite (α-FeOOH). J. Soil Sci. **35**, 381, **1984**.
96. GROSSL P. R., EICK M., SPARKS D. L., GOLDBERG S., AINSWORTH C. C. Arsenate and Chromate Retention Mechanisms on goethite 2. kinetic evaluation using a pressure jump relation technique. Environ. Sci. Technol. **31**, 321, **1997**.
97. WAYCHUNAS G. A., REA B. A., FULLER C.C., DAVIS J. A. Surface Chemistry of Ferrihydrite: Part 1 EXAFS studies of the geometry of coprecipitated and adsorbed arsenate. Geochim Cosmochim Acta **57**, 2251, **1993**.
98. MANCEAU A. The Mechanisms of anion adsorption on iron oxides: Evidence for the binding of arsenate tetrahedral on free Fe(O, OH)6 edges. Geochim. Cosmochim Ac. **59**, 3647, **1995**.
99. CARABANTE I., GRAHN M., HOLMGREN A., KUMPIENE J., HEDLUND J. Adsorption of As (V) on iron oxide nanoparticle films studied by *in situ* ATR-FTIR Spectroscopy. Colloids and Sufaces Eng. Aspects. **346**, 106, **2009**.
100. BORGGAARD O. K., RABEN-LANGE B., GIMSING A. L., STROBEL B. W. Influence of humic substances on phosphate adsorption by aluminium and iron oxides. Geoderma **127**, (3-4), 270, **2008**.
101. STREAT M., HELLGARDT K., NEWTON N.L. R. Hydrous ferric oxide as an adsorbent in water treatment Part 2. Adsorption studies. Process Safety Environ. Protection **86**, 11, **2008**.
102. SIMEONIDIS K., TRESINTSI S. , MARTINEZ-BOUBETA C., VOURLIAS G., TSIAOUSSIS I., STAVROPOULOS G., MITRAKAS M., ANGELAKERIS M. Magnetic separation of hematite coated Fe_3O_4 particles used as arsenic adsorbents. Chem. Eng. J. **168**, 1008, **2011**.
103. NAMDEO M., BAJPAI S. K. Investigation of hexavalentchromium uptake by synthetic magnetite nanoparticles. Elec. J. Environ. Agric. And Food Chemistry **7**, (7), 3082, **2008**.
104. AJOUYED O., HUREL C., AMMARI M., BEN ALLAL L., MARMIER N. Sorption of Cr (VI) onto natural iron and aluminium (oxy) hydroxides: Effects of pH, ionic strength and initial concentration. J. Hazard. Mater. **174**, 616, **2010**.
105. SINGH D. B., GUPTA G.S., PRASAD G., RUPAINWAR D. C. The Use of hematite for chromium (VI) removal. J. Environ. Sci. Health A **28**, (8), 1813, **1993**.
106. BAJPAI S.K., ARMO M.K. Equilibrium Sorption of hexavalent Chromium from aqueous solution using iron (III) loaded chitosan-magnetite nanocomposites as novel sorbent. J. Macromolecular Sci. Part A: Pure and Appl. Chemistry **46**, 510, **2009**.
107. ZHAO D., WANG X., YANG S., GUO Z., SHENG G. Impact of water quality parameters on the sorption of U (VI) onto hematite. J. Environ. Radioactiv. **103**, 20, **2012**.
108. LEFEVRE G., NOINVILLE S., FEDOROFF M. Study of Uranyl sorption onto hematite by in situ attenuated total reflectance-infrared spectroscopy. J. Colloid Interf. Sci. **296**, 608, **2006**.
109. VAUGHAN JR R. L., REED B.E. Modelling As(V) removal by iron oxide impregnated activated carbon using the surface complexation approach. Water Res. **39**, 1005, **2005**.
110. KENDELWICZ T., LIU P., DOYLE C. S., BROWN Jr G. E. Spectroscopic study of the reaction of aqueous Cr (VI) with Fe3O4 (I I I) surfaces. Surface Sci. **469**, 144, **2000**.
111. LENOBLE V., BOURAS O., DELUCHAT V., SERPAUD B., BOLLINGER JC. Arsenic Adsorption onto pillared clays and iron oxides. J. Colloid Interf. Sci. **225**, 52, **2002**.
112. GAO Y., MUCCI A. Individual and Competitive adsorption of phosphate and arsenate on goethite in artificial sea water. Chem. Geol. **199**, 91, **2003**.

113. SHERMAN D. M., RANDALL S. R. Surface complexation of arsenic (V) to iron (III) (hydr)oxides: Structural mechanism from ab initio geometries and EXAFS spectroscopy. Geochim. Cosmochim. Ac. **67**, (2), 4223, **2003**.
114. DELIYANNI E. A., BAKOYANNAKIS D. N., ZOUBOULIS A. I., MATIS K. A. Sorption of As(V) ions by akaganeite-type nanocrystals. Chemosphere **50**, 155, **2003**.
115. DUC M., LEFEVRE G., FEDOROFF M., JEANJEAN J., ROUCHAUD J.C., MONTEIL-RIVERA F., DUMONCEAU J., MILONJIC S. Sorption of anionic species on apatites and iron oxides from aqueous solution. J. Environ. Radioactiv. **70**, 61, **2003**.
116. REGENSPURG S., PEIFFER S. Arsenate and Chromate incorporation in schwertmannite. Appl. Geochem. **20**, 1226, **2005**.
117. LAKSHMIPATHIRAJ P., NARASIMHAN B.R. V., PRABHAKAR S., BHASKAR RAJU G. Adsorption of arsenate on synthetic goethite from aqueous solutions. J. Hazard. Mater. B **136**, 281, **2006**.
118. LAKSHMIPATHIRAJ P., NARASIMHAN B.R. V., PRABHAKAR S., BHASKAR RAJU G. Adsorption studies of arsenic on Mn-substituted iron oxide. J. Colloid Interf. Sci. **304**, 317, **2006**.
119. JIA Y., XU L., WANG X., DEMOPOULOS G.P. Infrared spectroscopic and X-ray diffraction characterization of the nature of adsorbed arsenate on ferrihydrite. Geochim. Cosmochim. Ac. **71**, 1643, **2007**.
120. LUENGO C., BRIGANTE M., AVENA M. Adsorption kinetics of phosphate and arsenate on goethite: A comparative study. J. Colloid Interf. Sci. **311**, 354, **2007**.
121. ZENG H., ARASHIRO M., GIAMMAR D.E. Effects of water chemistry and flow rate on arsenate removal by adsorption to an iron oxide-based sorbent. Water Res. **42**, 4629, **2008**.
122. YIN S., ELLIS D. E. DFT studies of Cr (VI) Complex adsorption on hydroxylated hematite (1102) surfaces. Surf. Sci. **603**, 736, **2009**.
123. MAMINDY-PAJANY Y., HUREL C., MARMIER N. ROMEO M. Arsenic adsorption onto hematite and goethite. C.R. Chimie **12**, 876, **2009**.
124. MULLER K., CIMINELLI V.S. T., SYLVA M. DANTAS S. A comparative study of As(III) and As(V) in aqueous solutions and adsorbed on iron oxy-hydroxides by Raman spectroscopy. Water Research **44**, 5660, **2010**.
125. YUSAN S.D., ERENTURK S. A. Sorption behaviours of uranium (VI) ions on α-FeOOH. Desalination **269**, 58, **2011**.
126. MAMINDY-PAJANY Y., HUREL C., MARMIER N., ROMEO M. Arsenic (V) adsorption from aqueous solution onto goethite, hematite, magnetite and zero-valent iron: Effects of pH, concentration and reversibility. Desalination **281**, 93, **2011**.
127. ZHU J., PIGNA M., COZZOLINO V., CAPORALE A. G., VIOLANTE A. Sorption of arsenite and arsenate on ferrihydrite: Effect of organic and inorganic ligands. J. Hazard. Mater. **189**, 564, **2011**.
128. LUTHER S., BORGFELD N., KIM J., PARSONS J.G. Removal of arsenic from aqueous solution: A study of the effects of pH and interfering ions using iron oxide nanomaterials. Microchemical J. Microc-01452(7pages). **2011**.
129. ZHANG Y., YANG M., HUANG X. Arsenic (V) removal with a Ce(IV) – doped iron oxide adsorbent. Chemosphere **51**, 945, **2003**.
130. HLAVAY J., POLYAK K., Determination of surface properties of iron hydroxide – coated alumina adsorbent prepared for removal of arsenic from drinking water. J. Colloid Interf. Sci. **284**, 71, **2005**.
131. KUNDU S., GUPTA A. K., Adsorption characteristics of As (III) from aqueous solution on iron oxide coated cement (IOCC). J. Hazard. Matter. **142**, 97, **2007**.
132. CHOWDHURY S.R., YANFUL E.K. Arsenic and chromium removal by mixed magnetite-maghemite nanoparticles and the effect of phosphate on removal. J. Environ. Manage. **91**, 2238, **2010**.
133. WAINIPEE W., WEISS D. J., SEPHTON M.A., COLES B.J., UNSWORTH C. and COURT R. The effect of crude oil on arsenate adsorption on goethite Water Res. **44**, 5673, **2010**.